

# Measurement of the Fragmentation Rates of Solvated Ions in Ion Electropray Thrusters

Catherine E. Miller\* and Paulo C. Lozano†

*Massachusetts Institute of Technology, Boston, MA, 02139, USA*

Ionic Liquid Ion Sources (ILIS) produce ion beams from ionic liquids and are the basis of ion electropray propulsion. ILIS beams are typically composed of single ions as well as ion clusters. The ion clusters are metastable and can break up inside the thruster, a phenomena referred to as fragmentation. Fragmentation within the acceleration region of the thruster is detrimental to the propulsive efficiency. Therefore it is imperative to understand the physics behind the fragmentation process. Unfortunately fragmentation is not well characterized and it has been experimentally shown that different ionic liquids produce ILIS beams with different amounts of fragmentation. In this work, the rates at which ion clusters break up were experimentally determined using retarding potential analysis. The beam energy distribution was measured using a retarding potential analyzer placed at several distances from the source. It was found that the rates are likely constant outside of the acceleration region. For a source voltage of 1820 V, the mean lifetime of the lightest ion cluster is approximately 1  $\mu$ s, which indicates that the solvated species are highly metastable. Improvements to the experimental apparatus and data analysis methods are required to increase the accuracy of the fragmentation rates. In future work, measurements close to the source will be obtained in order to better constrain the fit used to determine the rates.

## Nomenclature

$K_{bi}$	Kinetic energy of a broken ion, J
$q$	Ion charge, C
$V_0$	Source voltage, V
$m_{bi}$	Mass of broken ion, kg
$m_{pi}$	Mass of parent ion, kg
$V_B$	Voltage at which fragmentation occurs inside the acceleration region, V
$f_f$	Current fraction of dimers that fragment into monomers in field-free space
$f_{di,0}$	Initial current fraction of dimers that enter field-free space
$t$	Time, s
$R$	Fragmentation rate, $s^{-1}$
$d$	Distance between source and RPA, in or m
$v_{di}$	Dimer velocity, m/s
$m_{di}$	Mass of dimer, kg

## I. Introduction

Ion electropray thrusters use room temperature molten salts, called ionic liquids, as propellant. These liquids consist purely of positive and negative molecular, and sometimes atomic, ions. The strong Coulombic forces between the ions in the liquid results in negligible vapor pressures, making ionic liquids suitable for in-space applications.<sup>1</sup> Ionic liquids have moderate conductivity, approximately 1 Si/m,<sup>1</sup> which makes the

---

\*Graduate Research Assistant, Department of Aeronautics and Astronautics, 77 Mass Ave 37-307, and AIAA Member.

†Professor, Department of Aeronautics and Astronautics, 77 Mass Ave 37-401, and AIAA Member.

Pure Ionic Regime (PIR) more accessible than when using doped solvents.<sup>2</sup> Ions can be evaporated from the liquid surface through the application of strong electric fields. The free ions can be accelerated by the same electric potential to produce an ion beam with a few keV of energy. ILIS beams are useful for spacecraft propulsion as well as for Focused Ion Beam (FIB) etching and deposition.

Ion electrospray thrusters have the potential for propulsive efficiencies greater than 90%.<sup>3</sup> However the propulsive efficiency can be limited by the polydispersity of the ion beam.<sup>3,4</sup> Polydispersity arises when ions exit the thruster at different velocities, which has a negative effect on the efficiency.<sup>3,4</sup> This is a common occurrence in ion electrospray thrusters because they emit single ions as well as ion clusters of various masses.<sup>1</sup> When ions of the same charge but different masses are accelerated by the same electric potential, they exit the thruster at different final velocities. The situation is further complicated because the solvated species are metastable and can break apart mid-flight.<sup>5</sup> This process, called fragmentation, makes the ion beam no longer monoenergetic and further reduces the polydispersive efficiency.<sup>4</sup> Fragmentation is not a well-characterized process that requires further study due to its significant impact on ion electrospray thruster performance. The focus of this work is on the measurement of the fragmentation rates of the solvated ions, a quantity that has not yet been experimentally investigated. These measurements will help estimate the effective energy distribution of the solvated species, which drives the amount of fragmentation and will provide insight into the physics of the ion emission process.

## II. Ionic Liquid Ion Sources

In this work, a single emitter ionic liquid ion source was used. Figure 1 shows a single emitter ILIS. The

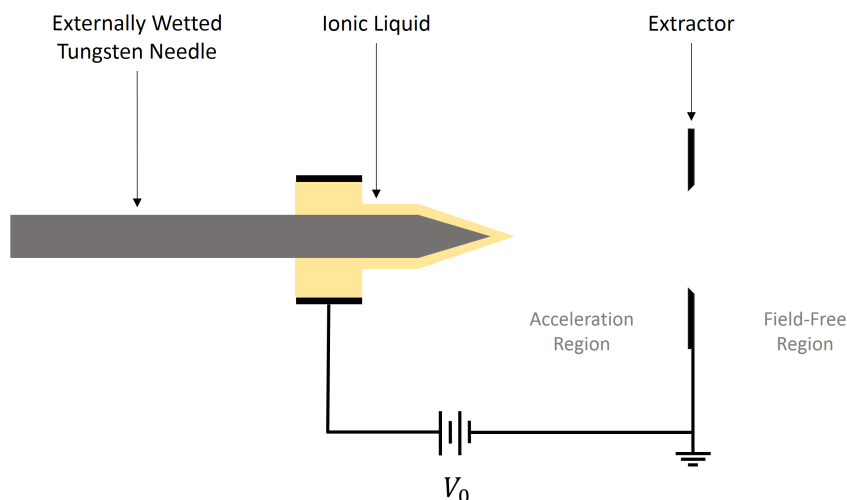


**Figure 1. Single emitter ILIS.**

emitter is an externally wetted, electrochemically etched, chemically roughened tungsten needle with a tip radius of curvature of approximately  $20 \mu\text{m}$ .<sup>6</sup> The needle is dipped in ionic liquid and a liquid reservoir is placed approximately 3 mm upstream from the tip. A stainless steel plate with a 1.6 mm aperture, called the extractor, is placed approximately  $500 \mu\text{m}$  from the tip of the needle. Approximately 1-2 kV, positive or negative polarity, applied between the liquid reservoir and the extractor is required to produce an ion beam.

When 1-2 kV is applied, the liquid surface at the tip of the needle is electrically stressed. The surface of the liquid collapses into a nearly conical structure similar to a Taylor Cone.<sup>7,8</sup> The sharpened liquid meniscus enhances the applied electric field and the field strength increases towards the tip of the cone. Within a few tens of nanometers of the tip, the field strength exceeds the required 1 V/nm needed to induce ion evaporation.<sup>1</sup> In a very localized region at the tip of the liquid cone, single ions as well as solvated species are evaporated. These ions are then accelerated towards the extractor and exit through the aperture, resulting in a 1-2 kV ion beam.

## A. Beam Composition and Fragmentation

Ionic liquid ion sources typically produce single ions and ion clusters.<sup>1</sup> The composition of the ion beam varies with the ionic liquid propellant.<sup>9</sup> Approximately 50% of an ILIS beam consists of single ions, referred to as monomers.<sup>1,6,9</sup> A dimer is a single ion attached to a single cation-anion pair, called a neutral. Dimers typically account for approximately 50% of the ILIS beam.<sup>1,6,9</sup> Highly solvated ions such as trimers, a single ion attached to two neutrals, or tetramers, a single ion attached to three neutrals, can be present in amounts typically less than 5%.<sup>1,6,9</sup> In this work EMI-BF<sub>4</sub> is used since it is the most well characterized and commonly used ionic liquid in ion electro spray thrusters. Figure 2 shows both positive and negative monomers and dimers for an EMI-BF<sub>4</sub> ILIS.

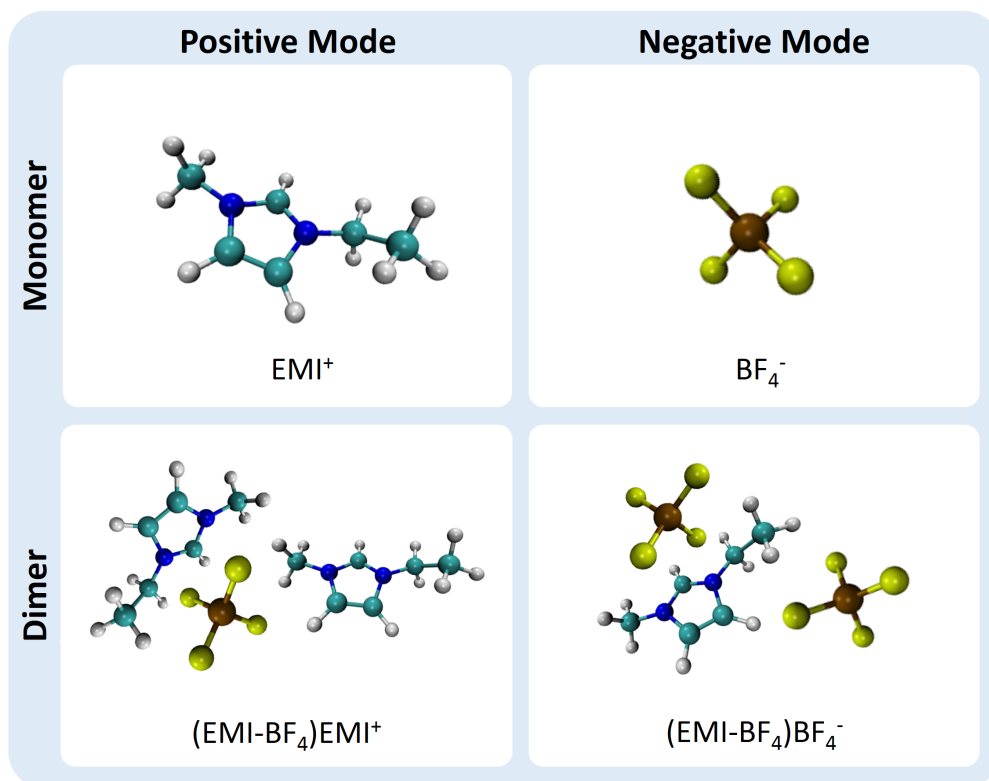


Figure 2. EMI-BF<sub>4</sub> monomers and dimers.<sup>4</sup>

The production and fragmentation of solvated species has a negative effect on ion electro spray thruster efficiency.<sup>4</sup> Single ions and solvated ions have the same charge and are accelerated through the same electric potential, but they have different masses, which means that they exit the thruster at different velocities. This results in an efficiency loss due to the non-zero polydispersity.<sup>3,4</sup> For example, an ILIS using EMI-BF<sub>4</sub> that produces half monomers and half dimers will have a polydispersive efficiency of approximately 94%.<sup>4</sup> Fragmentation of solvated species further reduces the polydispersive efficiency. A loss in propulsive efficiency occurs only when solvated ions break up within the acceleration region.<sup>4</sup> Despite the reduction in propulsive efficiency, the low energy fragmented ions play an important role in spacecraft neutralization during electro spray operation in space.<sup>10</sup> Solvated ions fragment into a less massive ion, called a broken ion, and a cluster of neutrals. For example, Figure 3 shows a negative dimer breaking up into a negative monomer. The broken ion is further accelerated by the electric potential, but the final kinetic energy is always less than the full accelerating potential energy.<sup>6</sup> The cluster of neutrals can no longer be accelerated by the electric field and it exits the thruster at low velocity. Since solvated species can break up anywhere with respect to the electric potential within the acceleration region, the broken ions and neutral clusters leave the thruster at a spread in velocities.<sup>4,6</sup> Thus fragmentation increases the polydispersity in the beam, which

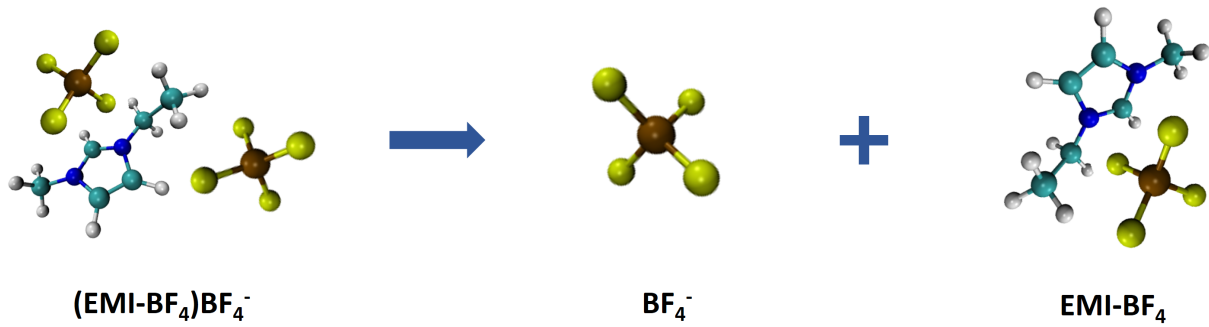


Figure 3. Fragmentation of an EMI-BF<sub>4</sub> negative dimer.<sup>4</sup>

reduces the efficiency. If 50% of the dimers break up in the acceleration region in the example mentioned previously, the polydispersive efficiency would be approximately 89%.<sup>4</sup>

The amount of fragmentation varies with the ionic liquid propellant, a relationship that is not well understood.<sup>4,6</sup> One important factor is the molecular complexity (ie: number of atoms) of the ions in the ionic liquid. It is hypothesized that solvated ions composed of complex molecules are less likely to fragment than solvated species composed of simple molecules.<sup>4</sup> Solvated ions are imparted with excess energy when they are extracted from the surface of the liquid, which may cause the ion cluster to break apart.<sup>4</sup> In principle, complex ions can redistribute the excess energy throughout their many bonds, leaving less energy to stretch the ion cluster apart.<sup>4</sup> Past experiments support this hypothesis;<sup>4-6,11,12</sup> however future experiments conducted under very controlled conditions using well-characterized, consistent instrumentation is needed. Another factor is the initial energy distribution of the solvated ions, which strongly affects the amount of fragmentation and may vary with the ionic liquid composition. The distribution of solvated ions that break up with respect to time may help indicate the characteristics of the initial energy distribution. The fragmentation rates in ILIS beams have not been measured before, so it is unknown if the rates are constant or variable in time. It is also unknown if 100% of the solvated species break up at some distance from the thruster. Measuring the amount of fragmented species at various distances from the ion source should provide an approximate shape of the initial energy distribution of the solvated ions.

## B. Beam Energy Distribution

ILIS beams with no fragmentation are monoenergetic with an energy corresponding to the acceleration potential. Unfortunately fragmentation is prevalent in ILIS beams, resulting in a monoenergetic population of unfragmented ions and a lower energy population of ion fragments. By measuring the beam energy distribution, it is possible to determine the amount of fragmented ions in the beam. Fragmentation can occur both in the acceleration region and outside of the acceleration region, also referred to as the field-free region. The energy distribution signatures from fragmentation in both regions are very distinguishable.

When a solvated ion breaks up in the field-free region, the energies of the broken ion and neutral cluster will always be the same for a given type of solvated ion. For example, when a dimer breaks up into a monomer in field-free space, the broken ion will always have the mass of a monomer and the velocity of a dimer. This means that the final kinetic energies of the fragmentation products of any dimer that breaks up in field-free space will be constant values. Eq. (1) shows the final kinetic energy of a broken ion produced by a fragmentation event in the field-free region:

$$\frac{K_{bi}}{qV_0} = \frac{m_{bi}}{m_{pi}} \quad (1)$$

where  $K_{bi}$  is the kinetic energy of the broken ion,  $V_0$  is the source potential,  $q$  is the ion charge,  $m_{bi}$  is the mass of the broken ion, and  $m_{pi}$  is the mass of the parent solvated ion.<sup>6</sup>

In the case of fragmentation in the acceleration region, the final kinetic energy of the broken ion and neutral cluster depends on the local value of the electric potential where the parent ion broke up. Eq. (2)

shows the final kinetic energy of a broken ion produced by a fragmentation event in the acceleration region:

$$\frac{K_{bi}}{qV_0} = \frac{m_{bi}}{m_{pi}} \left( 1 - \frac{V_B}{V_0} \left( 1 - \frac{m_{bi}}{m_{pi}} \right) \right) \quad (2)$$

where  $K_{bi}$  is the kinetic energy of the broken ion,  $V_0$  is the source potential,  $q$  is the ion charge,  $m_{bi}$  is the mass of the broken ion,  $m_{pi}$  is the mass of the parent solvated ion, and  $V_B$  is the local value of the electric potential where the ion broke up.<sup>6</sup>

Fragmentation in field-free space appears as sharp steps in the energy distribution, whereas fragmentation in the acceleration region appears as modest slopes. The energy distribution changes as a function of the distance from the source. The amount of fragmentation in the acceleration region will remain constant because the size of the acceleration region does not change. However the amount of fragmentation in the field-free region will increase with increasing distance from the source since the ions spend an increasing amount of time outside of the thruster. One of the most prominent features of an ILIS beam energy distribution is the sharp step corresponding to the fragmentation of dimers into monomers in field-free space. As the distance from the source increases, the height of this step should increase. By measuring the energy distribution at various distances, the amount of dimers that fragment into monomers in field-free space can be determined as a function of distance, which yields the fragmentation rates of dimers in this region.

### III. Experimental Methods

Retarding potential analysis was used to measure the energy distribution of a single emitter EMI-BF<sub>4</sub> ILIS. The energy distribution yields the amounts of fragmentation both inside and outside of the acceleration region. The amount of fragmentation as a function of distance can be used to estimate the fragmentation rates. In this work the RPA was placed at various distances from the source to obtain the energy distribution as a function of distance.

#### A. Retarding Potential Analysis

Retarding potential analysis (RPA) yields the energy distribution of ILIS beams, which can be used to determine the amounts of fragmentation. A diagram of a planar RPA is shown in figure 4. The RPA

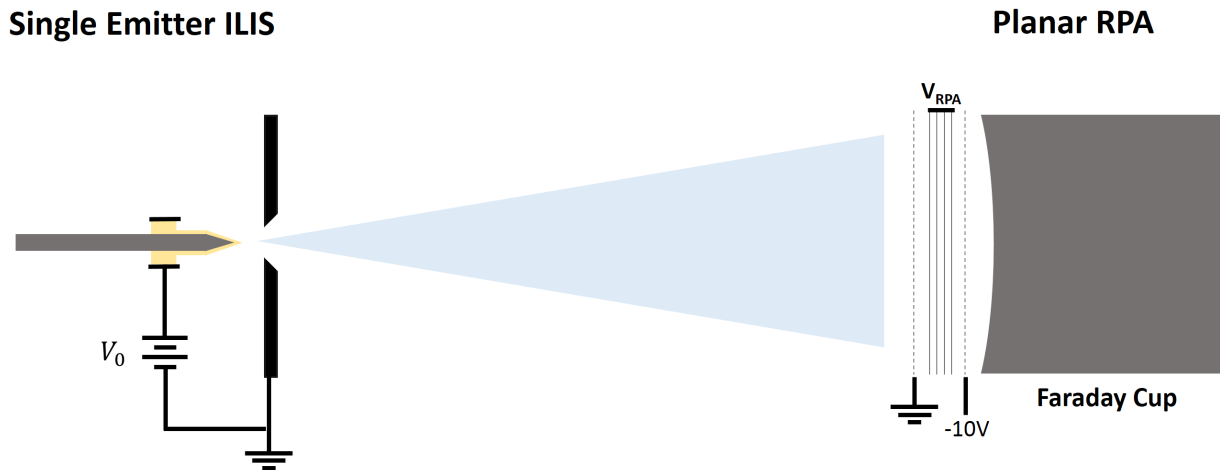


Figure 4. Planar retarding potential analyzer.

consists of a set of three semi-transparent, metallic grids and a metallic current collection surface. The first grid is grounded to ensure that the electric potential in the region between the extraction plate and the entrance to the RPA is at ground potential. The middle set of grids are the retarding grids which are varied from ground potential to  $V_0$ , the acceleration potential of the ion source. The last grid, called the electron

repelling grid, is biased to at least -10 V to keep any secondary electrons produced by ion impacts on the current collection surface from leaving the surface. The energy distribution of the ion beam is obtained by measuring the collected current as a function of the potential on the retarding grids. In the case of a beam with no fragmentation, the full beam current is measured as the retarding grid voltage is increased from zero. When the retarding voltage reaches the source potential, the measured current drops to zero because all of the ions are stopped because their kinetic energies are equal to the source potential.

### 1. Fragmentation Features in RPA Measurements

Figure 5 shows idealized RPA measurements for an ILIS with and without fragmentation. Figure 5a clearly shows that the beam is monoenergetic with an energy corresponding to the acceleration potential. When there is fragmentation the beam is no longer monoenergetic. Figure 5b shows an idealized RPA measurement for an ILIS with fragmentation. The vertical steps for fragmentation in field-free space as well as the slopes

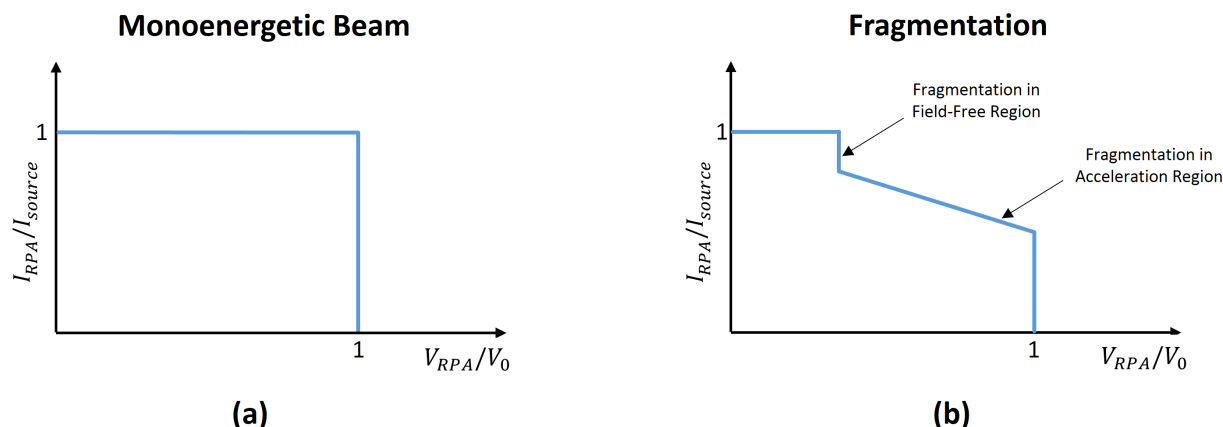


Figure 5. Idealized RPA signatures: monoenergetic beam (a), fragmentation (b).

for fragmentation in the acceleration region are easily identifiable.

### 2. RPA Design

There are many considerations when designing a retarding potential analyzer for the characterization of ILIS beams. The RPA can collect the full beam current or only a fraction of it. The beam can be electrostatically focused or left to expand spherically outward. The grid geometry can be planar, spherical, or something more exotic. The design goal for the RPA used in this work is to accurately measure the fragmentation signatures. In this case electrostatic lenses cannot be used to focus the beam since they require the application of electric fields that may induce fragmentation. Additionally the focal distance depends on the ion energy, so if the monoenergetic population is in focus at the collector, the lower energy fragmented ions will be out of focus.<sup>5</sup> Instead it is better to let the ion beam expand spherically outward. In order to make measurements that are representative of the energy properties of the full ion beam, the RPA must collect all of the current. This means that the RPA must be large in size in order to capture the full beam. Finally the grid geometry was chosen to be spherical because planar grids suffer from unwanted features known as spreading.

Spreading features in RPA measurements make it very challenging to measure the amount of fragmentation in each region accurately. Spreading arises from the fact that planar grids apply the retarding electric field axially. A planar RPA only needs to retard the axial velocity of the ions to stop them from reaching the collector. ILIS beams typically have a 20° half angle spread, which means that most of the ions travel off axis. A planar RPA will stop much of the ion population from reaching the collector at retarding voltages less than the kinetic energy of the ions since only a fraction of their kinetic energy is directed axially. Instead of measuring sharp steps corresponding to fragmentation in field-free space, the steps will be spread out and become harder to identify. The spreading features can be seen in figure 6a which shows planar RPA data for an EMI-BF<sub>4</sub> ILIS with a source voltage of 1872 V and a source current of 396 nA. Spherical grids avoid this problem because they apply the retarding electric field always parallel to the ion velocity direction. The

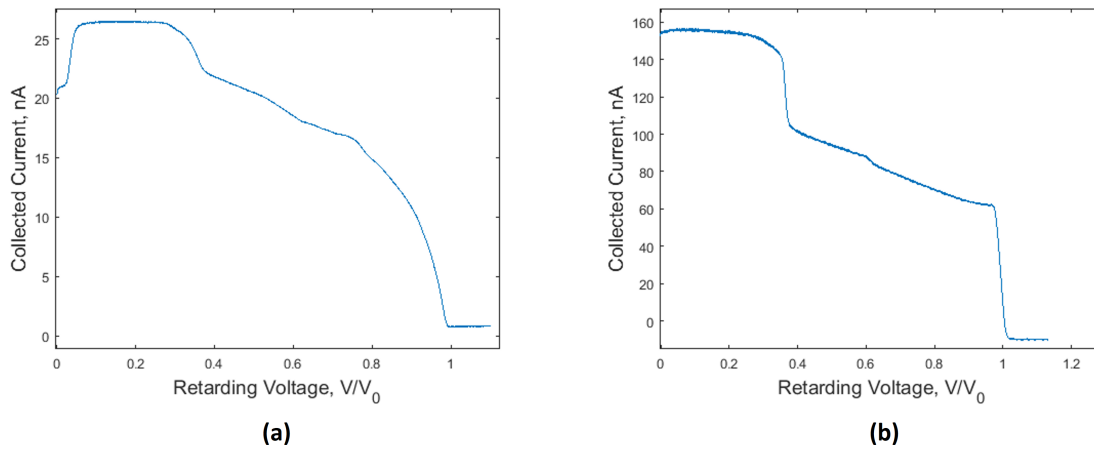


Figure 6. Planar (a) and spherical (b) RPA measurements for an EMI-BF<sub>4</sub> ILIS.

fragmentation features are much more distinct in the spherical RPA measurements shown in figure 6b. Here an EMI-BF<sub>4</sub> ILIS was operated at a source voltage of 1818 V with an emission current of 396 nA.

A schematic of the spherical RPA used in this work is shown in figure 7. The front grounded grid and retarding grid are both spherical with a radius of curvature of 3". The electron repelling grid, and the collector are planar. The mixed geometry design was selected since the manufacture of the spherical grids is

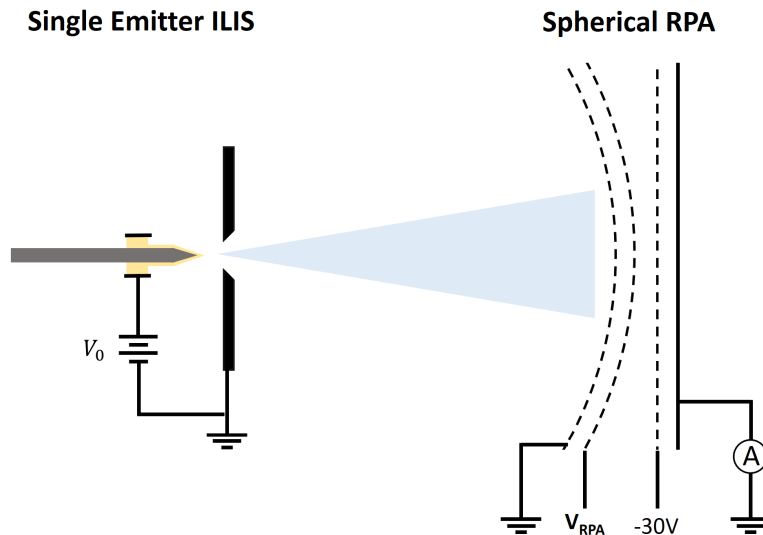


Figure 7. Spherical retarding potential analyzer.

quite challenging. It is less critical to have a spherical repelling grid and collector since the retarding field is applied through the combination of the front grounded grid and the retarding grid. This RPA was a first attempt at building and testing a spherical RPA, so the mixed geometry design was chosen for simplicity. The next design iteration of the RPA will have a spherical repelling grid and collector. The grids and collector plate were made of stainless steel and the RPA has a net transparency of 43%.

## IV. Results

The EMI-BF<sub>4</sub> ILIS was operated at voltages ranging from 1500-2150V in both the positive and negative modes. RPA measurements were taken with the electron repelling grid set to -30 V. The retarding grid voltage was controlled using a 10 second period triangular waveform. RPA measurements were taken at five different distances from the source ranging from 2-4". The optimum distance for minimum spreading is 3", which is equal to the radius of curvature of the spherical grids. The chamber was vented between each experiment since the RPA was moved to each position manually by hand. The ion source remained unmodified between experiments. This is not the most repeatable method, however it is adequate for the purpose of this work. Future experiments will allow the ion source to move relative to the RPA using a linear motion feed through.

### A. Current-Voltage Characteristics

The emitted current as a function of source voltage was measured before taking each set of RPA measurements. This was done to verify that the ion source was behaving in a similar manner for all experiments. Additionally the current-voltage characteristics help identify ranges of applied voltages for which the source current was stable. Figure 8 shows the current-voltage characteristics for both the positive and negative modes for all five possible RPA positions. Note that the emitted current was averaged into 5 V bins. The

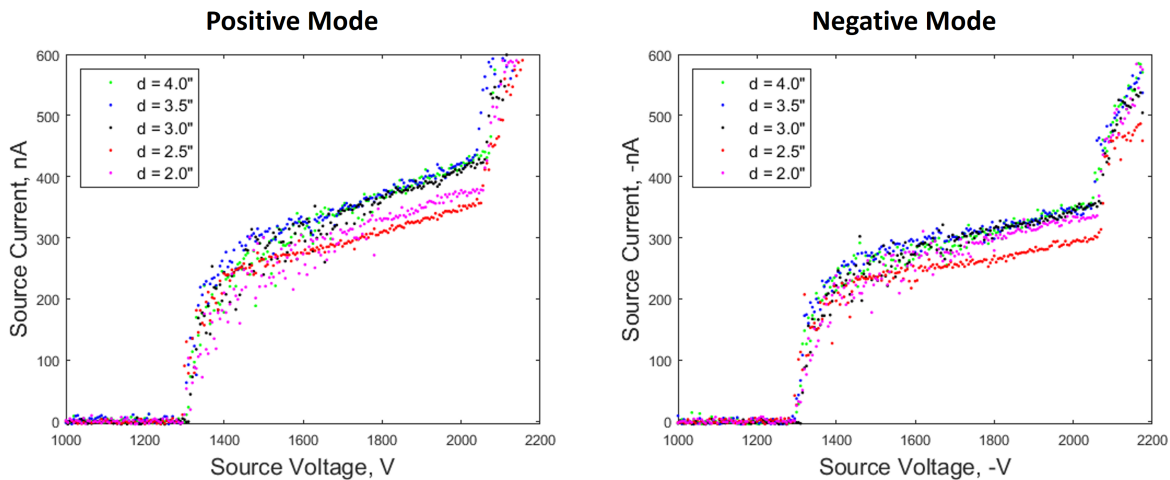


Figure 8. Current-voltage characteristics.

range of applied voltages for which the source was operating in a stable manner is 1800-1950 V for both positive and negative modes. RPA measurements for these voltages only were used to estimate the fragmentation rates.

The emitted current was also measured in-situ during the RPA measurements. The source voltage and current for each RPA measurement were averaged over the time that the RPA scan was taken. Figure 9 shows the in-situ current-voltage characteristics for both the positive and negative mode at all five RPA positions. It is clear that the current-voltage characteristics are consistent for most of the experiments; however the source was emitting less current when the RPA was 2.5" from the source. The data for which the RPA was 2.5" from the source was not used in estimating the fragmentation rates.

### B. Fragmentation in Field-Free Space

Several steps of data analysis are required to determine the amount of dimers that fragment into monomers in field-free space. First the collected current as a function of retarding voltage was corrected for the capacitive currents induced by the time-dependent voltage of the retarding grids. The capacitive currents were measured by taking an RPA scan when the source was off and were subtracted from the collected current for each RPA measurement.

Next the height of the step corresponding to the fragmentation of dimers into monomers in field-free space was determined. The collected current in the region where the step is located was fitted by a smoothing

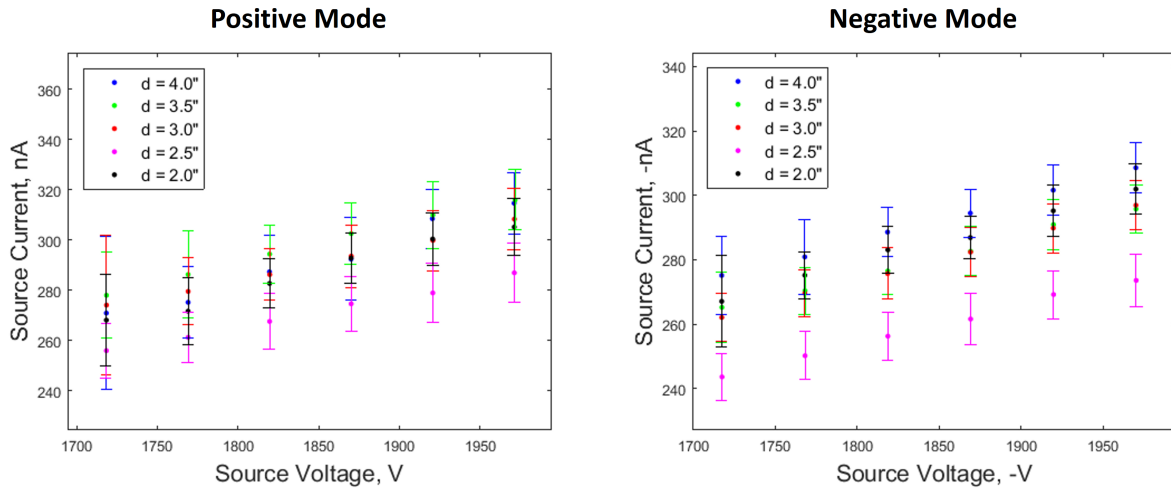


Figure 9. In-situ current-voltage characteristics.

spline function using MATLAB. Figure 10a shows the data and the fit of the step for a source potential of 1870 V, a source current of 294 nA, and an RPA distance of 3.0". The top and bottom of the step are

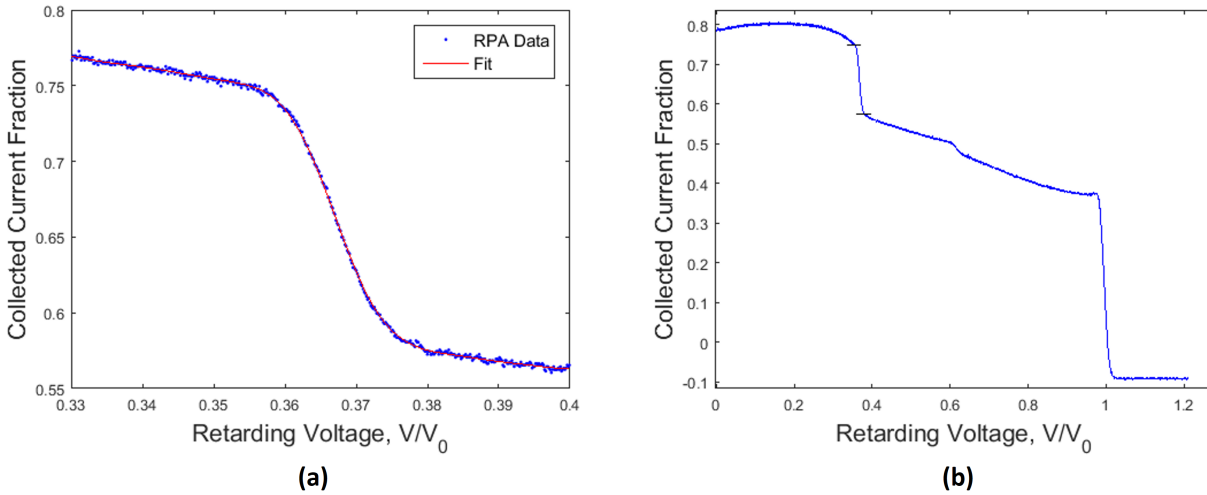


Figure 10. Step for fragmentation of dimers into monomers in field-free space.

marked by black horizontal lines in figure 10b. To determine the height of the step, the negative derivative of the RPA fit was computed and is shown in figure 11a. The negative derivative does not go to zero to the left and right of the step, which is due to fragmentation in the acceleration region. The offset from zero was determined by averaging the wings of the distribution shown in figure 11a. The offset was removed from the negative derivative of the RPA fit and the result was fitted with a smoothing spline, shown in figure 11b. The voltages for which the smoothed negative derivative of the fit equals one fifteenth of the peak value of the distribution were chosen to define the step. The intersection of the black horizontal lines and the distribution in figure 11b mark the top and bottom of the step. The height of the step was found by subtracting the current at the bottom of the step from the current at the top of the step.

In order to compare the step heights across all experiments, the current fraction of the step was calculated. For the positive mode, the top of the RPA curve was defined to be where the current levels off around  $V/V_0 = 0.1$ . In the negative mode the top of the RPA curve was taken to be the top of the step since the current increases as the retarding voltage goes to zero. This is likely an effect from secondary electrons and does not represent the ion energy distribution. The bottom of the RPA curve was defined as the current level where the retarding voltage exceeds the applied potential by approximately 50-100 V. The total collected

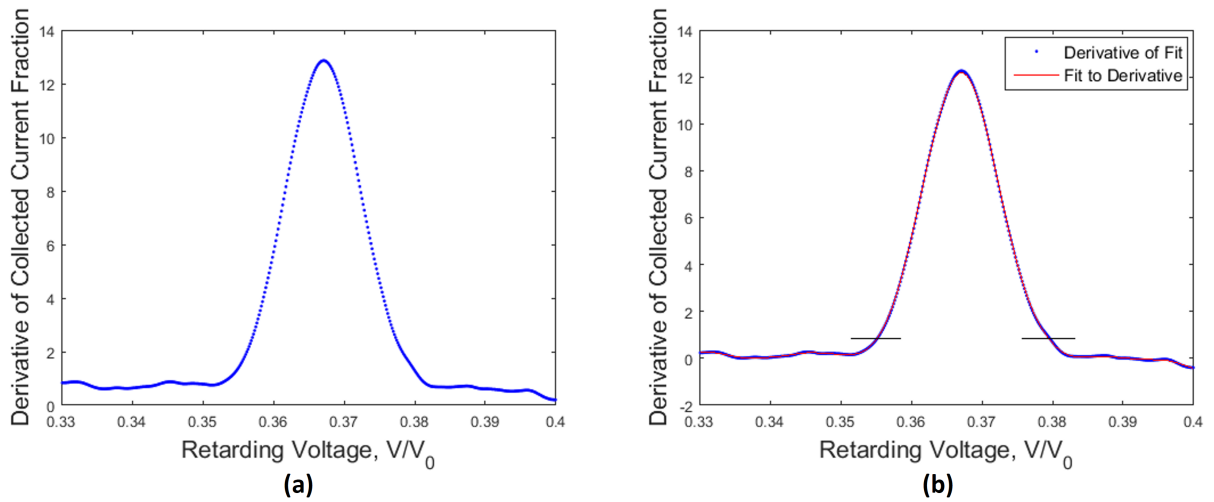


Figure 11. Fragmentation step height determination.

current was computed by subtracting the current at the bottom of the RPA curve from the current at the top of the RPA curve. The current fraction of dimers that fragment into monomers in field-free space was calculated by dividing the step height by the total collected current.

Figure 12 shows the current fraction of dimers that fragment into monomers in the field-free region as a function of the RPA position for various source voltages. The fragmentation current fraction increases

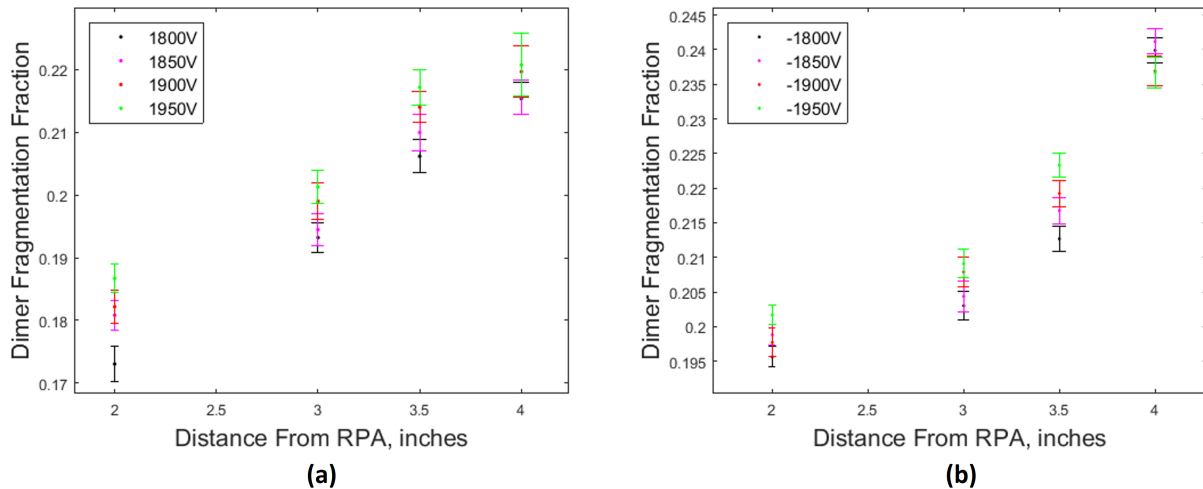


Figure 12. Current fraction of dimers that fragment in field-free space.

with increasing distance from the source, as expected. The fragmentation current fraction increases nearly linearly in the region sampled for the positive mode. For the negative mode, the fragmentation current fraction increases in a somewhat nonlinear manner in the region sampled. An additional observation is that the fragmentation current fraction is generally higher for higher source voltages. If the fragmentation rates were the same for all source voltages, one would expect to measure less fragmentation at higher voltages since the ions travel faster and spend less time in the field-free region. Instead the fragmentation rates must increase with increasing source voltage. This makes sense because the solvated species are imparted with more energy when higher source voltages are applied, which makes them more susceptible to fragmentation.

### C. Fragmentation Rates

If the rate of fragmentation remains constant in time, the amount of dimers that fragment in field-free space can be approximated by Eq. 3:

$$f_f = f_{di,0} \left(1 - e^{-Rt}\right) \quad (3)$$

where  $f_f$  is the current fraction of dimers that fragment into monomers in field-free space,  $f_{di,0}$  is the initial current fraction of dimers that enter the field-free region,  $t$  is time, and  $R$  is the constant fragmentation rate. The fragmentation current fraction as a function of distance can be described by Eq. 4:

$$f_f = f_{di,0} \left(1 - e^{-R\frac{d}{v_{di}}}\right) \quad (4)$$

where  $f_f$  is the current fraction of dimers that fragment into monomers in field-free space,  $f_{di,0}$  is the initial current fraction of dimers that enter the field-free region,  $d$  is the distance between the source and the RPA,  $v_{di}$  is the velocity at which dimers exit the source, and  $R$  is the constant fragmentation rate.

The velocity at which dimers exit the ion source is given by Eq. 5:

$$v_{di} = \sqrt{\frac{2qV_0}{m_{di}}} \quad (5)$$

where  $v_{di}$  is the velocity of a dimer,  $q$  is the ion charge,  $V_0$  is the source voltage, and  $m_{di}$  is the mass of a dimer.

The fragmentation current fraction in figure 12 can be fitted using Eq. 4. Theoretically the current fraction of dimers that fragment into monomers in field-free space should be zero at the extractor plate since the ions have not yet entered the field-free region. While this is not a measured data point, it was included in the fit. In the future, RPA measurements closer to the source will be made to better constrain the fit used to estimate the fragmentation rates. Only data from the positive mode was fitted since the results for the negative mode appear to be affected by the secondary electron currents and require further data analysis and correction. Figure 13 shows the fit for a source voltage of 1820 V. The fit parameters with 95% confidence

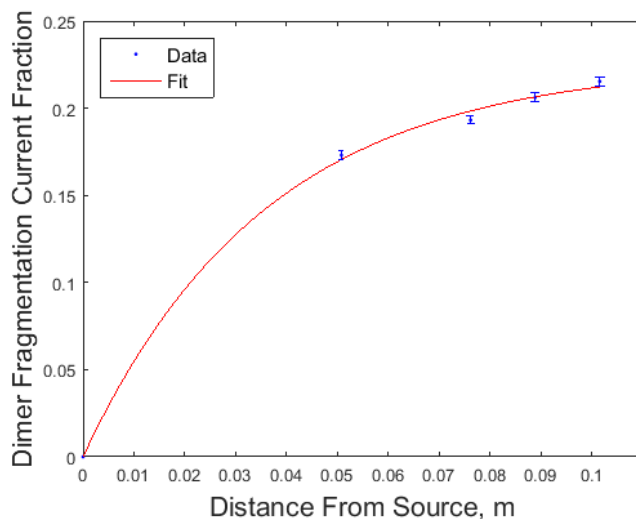


**Figure 13. Fragmentation rate determination.**

bounds are  $f_{di,0} = 0.2257$  (0.205, 0.2464) and  $R = 0.9349$  (0.6383, 1.2317)  $\mu s^{-1}$  with an R-squared value of 0.9986. The mean lifetime of the positive dimers in field-free space is approximately 1  $\mu s$ , which indicates that they are highly metastable.

The initial current fraction of dimers that enter field-free space determined by the fit is in good agreement with experimental results. Time of flight (TOF) mass spectrometry measurements were taken after the retarding potential analysis measurements. The ion source was not modified between the experiments. The TOF detector is placed approximately 73 cm from the source and has an acceptance half angle less than  $1^\circ$ .<sup>6</sup> TOF measurements were acquired for source voltages of 2.28 - 2.54 kV since the signal at the TOF detector

was too low at lower source voltages. The current fraction of dimers that survived the acceleration region was found to be approximately 0.242 - 0.284. Considering that the source was operating at much higher voltages than for the RPA measurements and that the TOF detector does not sample the full beam, this result is in reasonable agreement with the estimate from the fit of the RPA data.

## V. Conclusions and Future Work

In this work, a spherical retarding potential analyzer was used to measure the energy distribution of an EMI-BF<sub>4</sub> single emitter ILIS. In order to determine the fragmentation rates, the energy distribution was measured at various distances from the source. The current fraction of dimers that break up into monomers in the field-free region was extracted from the energy distribution. The rate at which dimers fragment into monomers was estimated by fitting a constant rate equation to the fragmentation current fraction as a function of the RPA distance. For a source voltage of 1820 V, the mean lifetime of dimers in the field-free region is approximately 1  $\mu$ s. This indicates that the solvated species are strongly metastable and do not survive for long after being emitted from the source. It was also determined from the fit that the current fraction of dimers that survive the acceleration region is approximately 0.20 - 0.25, which is in reasonable agreement with the time of flight measurements taken after the RPA experiments.

In future work, the fragmentation rates will be measured using a system that will provide more robust data over a wider range of distances. The RPA will be of a full spherical design instead of the mixed geometry used in this work. Additionally the ion source will be mounted on a linear stage so that the distance between the source and the RPA can be varied without venting the vacuum chamber. This configuration will allow for RPA measurements to be taken at distances much closer to the source, which are required to better constrain the fit and will help determine if the fragmentation rates are approximately constant in time. A model to account for the currents caused by secondary electrons is currently under development and will be used to correct the RPA measurements in the future. The negative mode measurements are more strongly affected by secondary electrons, so in this work it was not possible to estimate the fragmentation rates for the negative mode. The model will be critical in extracting the ion beam energy distribution from the RPA data, which will allow for the determination of the fragmentation rates in both polarities. With these improvements to the experimental apparatus and data analysis methods, the fragmentation rates of solvated ions in both the positive and negative modes will be determined with higher accuracy.

## Acknowledgments

This work was supported by a NASA Space Technology Research Fellowship. The authors would also like to thank other agencies of the US Government. Catherine Miller thanks Amy Vanderhout for her hard work designing and building the spherical RPA.

## References

- <sup>1</sup>Lozano, P., and Martinez-Sanchez, M., "Ionic Liquid Ion Sources: Characterization of Externally Wetted Emitters," *Journal of Colloid and Interface Science*, Vol. 282, No. 2, Feb. 2005, pp. 415-421.
- <sup>2</sup>Garoz, D., Bueno, C., Larriba, C., Castro, S., Romero-Sanz, I., Fernandez de la Mora, J., Yoshida, Y., and Saito, G., "Taylor Cones of Ionic Liquids from Capillary Tubes as Sources of Pure Ions: The Role of Surface Tension and Electrical Conductivity," *Journal of Applied Physics*, Vol. 102, No. 6, Sept. 2007, pp. 064913.
- <sup>3</sup>Lozano, P., and Martinez-Sanchez, M., "Efficiency Estimation of EMI-BF<sub>4</sub> Ionic Liquid Electrospray Thrusters," *The 41<sup>st</sup> AIAA/ASME/SAE/ASEE Joint Propulsion Conference & Exhibit*, Tuscon, AZ, 2005.
- <sup>4</sup>Coles, T., and Lozano, P., "Investigating Efficiency Losses from Solvated Ion Fragmentation in Electrospray Thruster Beams," *The 49<sup>th</sup> AIAA/ASME/SAE/ASEE Joint Propulsion Conference & Exhibit*, San Jose, CA, 2013.
- <sup>5</sup>Lozano, P., "Energy Properties of an EMI-Im Ionic Liquid Ion Source," *Journal of Applied Physics D*, Vol. 39, No. 1, Jan. 2006, pp. 126-134.
- <sup>6</sup>Miller, C., *On the Stability of Complex Ions in Ionic Liquid Ion Sources*," Master's Thesis, Massachusetts Institute of Technology, 2015.
- <sup>7</sup>Taylor, G., "Disintegration of Water Drops in an Electric field," *Proceedings of the Royal Society of London. Series A, Mathematical and Physical Sciences*, Vol. 280, No. 1382, 1964, pp. 383-397.
- <sup>8</sup>Coffman, C., *Electrically-Assisted Evaporation of Charged Fluids: Fundamental Modeling and Studies on Ionic Liquids*," Doctoral Thesis, Massachusetts Institute of Technology, 2016.
- <sup>9</sup>Legge, R., and Lozano, P., "Electrospray Propulsion Based on Emitters Microfabricated in Porous Metals," *Journal of Propulsion & Power*, Vol. 27, No. 2, March 2011, pp. 485-495.

<sup>10</sup>Mier-Hicks, F., and Lozano, P., "Spacecraft Charging Characteristics Induced by the Operation of Electro spray Thrusters," *Journal of Spacecraft Propulsion and Power* (submitted for publication).

<sup>11</sup>Fedkiw, T., and Lozano, P., "Development and Characterization of an Iodine Field Emission Ion Source for Focused Ion Beam Applications," *Journal of Vacuum Science & Technology: Part B-Microelectronics & Nanometer Structures*, Vol. 27, No. 6, 2009, pp. 2648-2653.

<sup>12</sup>Coles, T., Fedkiw, T., and Lozano, P., "Investigating Ion Fragmentation in Electro spray Thruster Beams," *The 48<sup>th</sup> AIAA/ASME/SAE/ASEE Joint Propulsion Conference & Exhibit*, Atlanta, GA, 2012.